PERGAMON

International Journal of Heat and Mass Transfer 43 (2000) 653–663

International Journal of HEAT and MASS TRANSFER

www.elsevier.com/locate/ijhmt

Effect of interface thermal resistance on heat transfer in a composite medium using the thermal wave model

Whey-Bin Lor, Hsin-Sen Chu*

Department of Mechanical Engineering, National Chiao Tung University, Hsinchu 300, Taiwan

Received 10 December 1998; received in revised form 18 May 1999

Abstract

This study analyzes how interface resistance affects heat transfer in a two-layered composite media under an incident pulse energy exerting on the exterior surface of one layer by using the hyperbolic heat conduction equation. The incident energy is absorbed and a pulse width temperature wave is generated within the skin depth of the first layer, which subsequently emanates to the second layer. Reflection and transmission occur when the initial pulse wave impacts the contact surface of the dissimilar material. In addition, the radiation-boundary-condition model based on Acoustic Mismatch Model or Diffuse Mismatch Model is used to predict the interface resistance. Analysis results indicate that the reflection–transmission combination phenomena strongly depend on the interface condition. Moreover, the thermal resistance restricts the energy transmission across the interface, creating a temperature difference at the interface and ultimately alerting the reflected wave feature. Our results further demonstrate that the critical thermal resistance magnitude to approach the perfect contact condition varies with the two-layered properties ratio and the absorption skin depth.

Keywords: Thermal wave model; Interface thermal resistance; Acoustic Mismatch Model; Diffuse Mismatch Model

1. Introduction

Interface thermal resistance profoundly influences the design and performance of a variety of devices making use of composite materials such as thin-film superconductors, micro-electronics layers package, fins, as well as numerous applications. Most analyses of heat transfer in a composite media treat conduction as a diffusion process which is related through Fourier's law. Those results confirm that the interface resistance seriously affects the heat transfer mechanism [1–3]. Fourier's law analysis suggests that an infinite speed of propagation of the thermal wave yields reliable results under most circumstances. However, recent investigations involving an extremely low temperature near absolute zero, extremely short transient duration, microstructures, and extremely high-rate change of temperature or heat flux have indicated that the heat propagation velocity under such circumstances becomes finite and dominant [4–7].

While considering the finite speed of wave propagation, Cattaneo [8] and Vernotte [9] separately proposed a modified heat flux model in the form of

$$\boldsymbol{q}(\boldsymbol{r},t+\tau) = -k\nabla T(\boldsymbol{r},t) \tag{1}$$

Based on the collision theory of molecules, the relaxation time τ is approximated to α/c^2 [10]. Clearly, for $\tau = 0$, Eq. (1) reduces to the classical diffusion theory,

* Corresponding author. Tel.: +886-3-5712121; fax: +886-3-5727930.

E-mail address: hschu@cc.nctu.edu.tw (H.S. Chu).

0017-9310/00/$ - see front matter
PII: S0017-9310(99)00178-7

Nomenclature

c	thermal wave speed
C_p	specific heat capacity
e	thermal incident energy
h	Planck's constant
k	thermal conductivity
k_B	Boltzmann constant
q	heat flux
$\boldsymbol{q}$	heat flux vector
$\boldsymbol{r}$	position vector
Q	total energy
t	time
T	temperature
T_0	initial temperature
$\bar{v}$	sound velocity
W	characteristics variable
x	position
ρ	density
α	thermal diffusivity
τ	relaxation time
λ	eigenvalue
ε_d	non-dimensional incident energy
δx	skin depth
κ	constant; see Eq. (5)
Γ	constant; see Eq. (5)
ΔT_c	temperature difference at interface, $T_{1c} - T_{2c}$
λ_d	dominant phonon wavelength
σ	mean interfacial roughness

Superscripts

$*$	dimensionless variable
n, $n+1$	time levels n and $n+1$
iter	iteration

Subscripts

1	layer 1
2	layer 2
c	interface
i	control volume index
$i \pm 1/2$	value at control volume faces
j	layer index
r	ratio

leading to an infinite propagation velocity. When Eq. (1) is used in a local energy balance, a hyperbolic equation is derived. Temperature fields obtained from hyperbolic heat conduction equation display wavelike characteristics that the traditional diffusion theory can not predict [11]. Recently, Mitra et al. [12] demonstrated that the temperature in a biological material is directly validating the hyperbolic natural of heat conduction with the non-Fourier predictions. In addition, the time lag between heat flux and the temperature gradient is related to the microscopic heat transfer behavior when the response time becomes extremely short [13]. Tzou [13] collected the following heat transfer models on a microscopic basis: thermal wave model, two-step model, phonon scattering model, and phonon radiative transfer model. Recently, Chen [14] proposed a model based on acoustic wave propagation for the phonon transport across a thin film. The thermal wave theory can be derived from the two-step model [15,16] and phonon radiative transfer model [17] for acoustically thick films. Other investigators have applied the thermal wave model to heat transfer in thin film conductors [18,19].

For engineering applications of thermal wave theory, Özisik and Tzou [20] thoroughly reviewed thermal wave propagation which included the sharp wave front and rate effects, thermal shock phenomenon, and thermal resonance phenomena. Various analytical methods have been proposed to elucidate the reflection, refraction, and transmission of thermal waves across a material interface. Frankel et al. [21] proposed a flux formulation to investigate the thermal waves in a composite media with a perfect contact interface. Tzou [22] performed harmonic analysis to examine the reflection and refraction thermal wave patterns from a surface and an interface between dissimilar materials. Previous investigations did not consider thermal resistance at the interface. Bai and Lavine [23] treated thermal resistance as a jump boundary condition of a thin layer. The new boundary conditions significantly affect the thermal wave solution [23,24]. However, the reflection and transmission phenomena related to the properties of each layer in the composite media [21], which can not be accurately predicted using a single layer with a jump boundary condition. To our knowledge, no work has thoroughly investigated reflection/transmission of thermal wave in a composite media with interface resistance.

Little [25] predicted the thermal resistance by treating the phonons as plane waves and, in doing so, proposed the acoustic mismatch model (AMM). An underlying assumption of the AMM is that no scattering occurs at the interface. Swartz and Pohl [26] not only assumed that diffuse scattering destroys acoustic effects at interface, but also proposed the diffusive mismatch model (DMM) as well. The AMM is applicable when $\lambda_d/\sigma \gg 1$, where λ_d is the dominant phonon wavelength, and σ is the mean interfacial roughness.

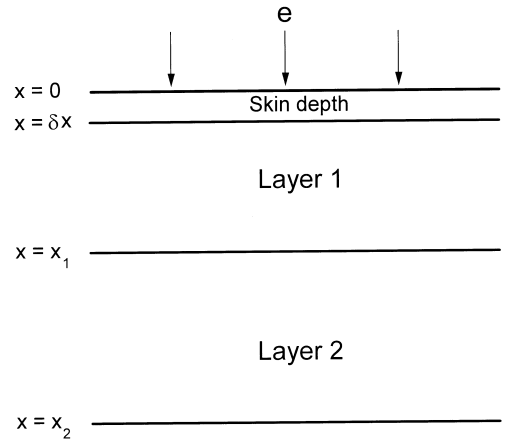

Fig. 1. Schematic diagram of the physical system.

However, when $\lambda_d/\sigma \leq 1$ the DMM should be employed [3,26]. Both models are in the same form as the radiation boundary condition, where the heat flow across the interface is proportional to the difference of the fourth power of the temperature on each side of the interface. In this study, we use the radiation-boundary-condition at the interface, which can be applied to either AMM or DMM, to consider the interface resistance. Also examined herein is how thermal resistance affects the wave propagating in a composite media. Analysis results indicate that the thermal resistance restricts the energy transmission across the interface, thereby influencing the wave patterns and their related strengths significantly.

2. Physical model and theoretical analysis

Fig. 1 shows the composite medium which consists of two different materials in layer 1 and layer 2. A pulsed incident energy exerts itself on the front surface of layer 1 and is absorbed within a skin depth of δx of layer 1. This system is highly promising for advanced semiconductor processing or laser annealing [27–30]. At time $= 0^+$, the thermal energy within δx is released and then emanates into the second layer.

By applying the Taylor's series expansion to $\boldsymbol{q}$ in Eq. (1) with respect to τ, the linearized constitutive equation and energy conservation equations are written as

$$q(x,t) + \tau \frac{\partial q(x,t)}{\partial t} = -k\nabla T(x,t). \tag{2}$$

$$\rho C_p \frac{\partial T(x,t)}{\partial t} + \nabla \cdot q(x,t) = 0. \tag{3}$$

When the radiation-boundary-condition model is employed, the continuity of interface heat flux becomes [25,26]

$$q_{1c} = q_{2c} = \kappa\left(T_{1c}^4 - T_{2c}^4\right) \tag{4}$$

where

$$\kappa = \frac{2\pi k_B^4 \Gamma}{h^3 \bar{v}^2}\left(\frac{\pi^4}{15}\right) \tag{5}$$

The most important constant is Γ, a function of the material properties of the two media in contact, which can be obtained if the density ratio and the sound velocity ratio of two media are known [25]. A large value of Γ represents a high transmission across the interface, i.e., a low boundary resistance. Eqs. (4) and (5) can be applied to both AMM and DMM, with the exception of a different value of Γ in a different model. The DMM predicts a larger value of Γ than AMM [26].

For convenience, in the subsequent analysis, the non-dimensional variables are defined in the transformed system as follows:

$$x^* = \frac{c_1 x}{2\alpha_1}, \quad t^* = \frac{c_1^2 t}{2\alpha_1}, \quad T_j^* = \frac{T_j - T_0}{T_0}, \quad q_j^* = \frac{\alpha_1 q_j}{T_0 k_1 c_1}, \quad \kappa^* = \frac{\kappa T_0^3 \alpha_1}{k_1 c_1} \tag{6}$$

and the dimensionless property ratios

$$\alpha_j^* = \frac{\alpha_j}{\alpha_1}, \quad \tau_j^* = \frac{\tau_j}{\tau_1}, \quad k_j^* = \frac{k_j}{k_1} \tag{7}$$

where $j = 1$ and 2 represent layer 1 and layer 2, respectively. Clearly, we have $\alpha_1^* = \tau_1^* = k_1^* = 1$. The energy equation and non-Fourier constitutive equation are expressed in terms of the above dimensionless variables as (with asterisks omitted)

$$\frac{\partial T_j}{\partial t} + \frac{1}{k_j}\frac{1}{\alpha_j}\frac{\partial q_j}{\partial x} = 0 \tag{8}$$

$$\frac{\partial q_j}{\partial t} + \frac{k_j}{\tau_j}\frac{\partial T_j}{\partial x} = -2\frac{1}{\tau_j} q_j \tag{9}$$

The non-Fourier constitutive equation along with the energy equation for each layer can be written in dimensionless vector form as

$$\frac{\partial \boldsymbol{U}_j}{\partial t} + \frac{\partial \boldsymbol{F}_j}{\partial x} = \boldsymbol{S}_j, \tag{10}$$

where

$$\boldsymbol{U}_j = \begin{Bmatrix} T_j \\ q_j \end{Bmatrix}, \quad \boldsymbol{F}_j = \begin{Bmatrix} \frac{1}{k_j}\frac{1}{\alpha_j} q_j \\ \frac{k_j}{\tau_j} T_j \end{Bmatrix}, \quad \boldsymbol{S}_j = \begin{Bmatrix} 0 \\ -2\frac{1}{\tau_j} q_j \end{Bmatrix}. \tag{11}$$

Eq. (10) can be written

$$\frac{\partial \boldsymbol{U}_j}{\partial t} + [A]_j \frac{\partial \boldsymbol{U}_j}{\partial x} = \boldsymbol{S}_j \tag{12}$$

and the Jacobian matrices are

$$[A]_j = \frac{\partial \boldsymbol{F}_j}{\partial \boldsymbol{U}_j} \tag{13}$$

Then, $[A]_j$ can be diagonalized through the eigenvectors

$$[A]_j = [R]_j [\lambda]_j [R]_j^{-1} \tag{14}$$

where λ denotes the diagonal matrices consisting of two eigenvalues of $[A]$ for each layer. Superscript -1 represents the inverse eigenmatrix. The diagonal matrices and the right eigenmatrices reveal that

$$[\lambda]_j = \begin{bmatrix} -\left(\frac{\alpha_j}{\tau_j}\right)^{1/2} & 0 \\ 0 & \left(\frac{\alpha_j}{\tau_j}\right)^{1/2} \end{bmatrix} \tag{15}$$

$$[R]_j = \begin{bmatrix} 1 & 1 \\ -k_j\left(\frac{1}{\alpha_j}\frac{1}{\tau_j}\right)^{1/2} & k_j\left(\frac{1}{\alpha_j}\frac{1}{\tau_j}\right)^{1/2} \end{bmatrix} \tag{16}$$

The interface condition of Eq. (4) becomes the dimensionless form of

$$q_{1c} = q_{2c} = \kappa\left[(T_{1c}+1)^4 - (T_{2c}+1)^4\right] \tag{17}$$

The initial state of the medium is taken at the equilibrium temperature T_0. Thus, the dimensionless initial conditions are given as

$$t = 0, \quad T = q = 0. \tag{18}$$

At time $= 0^+$, the thermal energy symbol ε_d of width δx is released. Immediately after the release of the thermal disturbance, leading to an additional initial condition for temperature

$$\int_0^{\delta x} T \, dx = \varepsilon_d, \text{ i.e.}$$

$$T = \begin{cases} \frac{\varepsilon_d}{\delta x}, & 0 \le x \le \delta x \\ 0, & \text{otherwise} \end{cases} \text{ for } t = 0^+ \tag{19}$$

$$\varepsilon_d = \frac{e c_1}{2\rho_1 C_{p1} \alpha_1 T_0} \tag{20}$$

The above equations are now considered subject to the insulated exterior surfaces.

3. Numerical method

This study adopts the characteristics-based numerical method developed by Yang [31] to solve the system of equations, which resolves the thermal wave without introducing oscillation or dissipation. First, multiply Eq. (12) by $[R]_j^{-1}$, then obtain

$$\frac{\partial \boldsymbol{W}_j}{\partial t} + \frac{\partial \boldsymbol{M}_j}{\partial x} = \boldsymbol{G}_j \tag{21}$$

where

$$[W]_j = [R]_j^{-1} \cdot [U]_j, \quad [M]_j = [\lambda]_j \cdot [W]_j,$$

$$[G]_j = [R]_j^{-1} \cdot [S]_j \tag{22}$$

Now, the problem attempts to solve the characteristics variable $[W]$, instead of the original coupled equations for T and q. Then, Eq. (21) is expressed by the finite difference with the explicit formulation. Therefore, we have

$$\boldsymbol{W}_i^{\text{iter}} = \boldsymbol{W}_i^n - \frac{\Delta t}{\Delta x}\left(\boldsymbol{M}_{i+1/2}^n - \boldsymbol{M}_{i-1/2}^n\right) + \Delta t \boldsymbol{G}_i^{\text{iter}} \tag{23}$$

where $\Delta x = x_{i+1/2} - x_{i-1/2}$, and $\Delta t = t^{n+1} - t^n$. Superscript 'iter' denotes the iteration value at new time step of $(n+1)$.

The total variation diminishing scheme [31] is used to compute the characteristic variable $[W]$ of the interior points. Moreover, a simple and accurate numerical algorithm presented by Yeung and Lam [32] applying the Godunov method is employed to compute the $[W]$ value at the point next to the boundaries.

Initially, the interface temperatures of two layers (T_{1c} and T_{2c}) are in equilibrium with a dimensionless temperature of 0. Iterations between heat flux and temperature for all of the grids at each time step are proceeded with until the criterion of convergence is met. The T_{1c} and T_{2c} at time step n are used to calculate the interface heat flux for time step $(n+1)$. Based on this interface heat flux value, the new iteration T and q values of layer 1 are obtained. The interface heat flux is updated by the new iteration value of T_{1c}. Then,

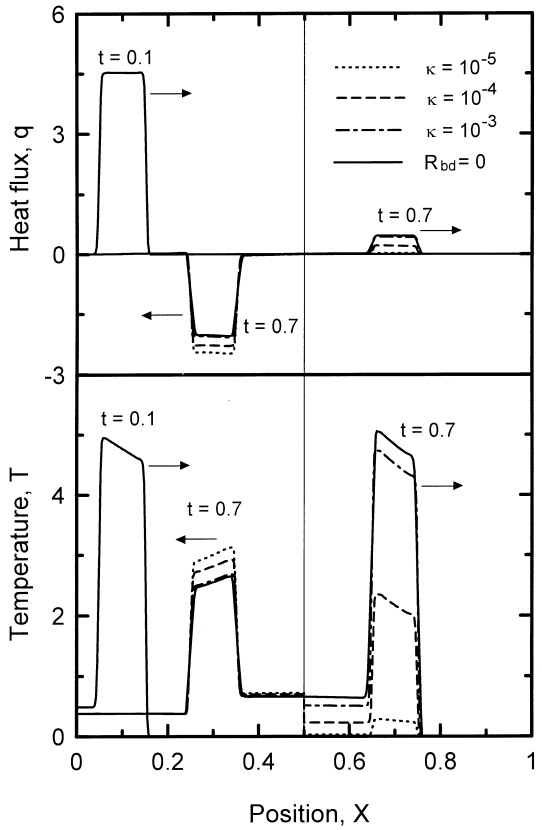

Fig. 2. Heat flux and temperature distributions at $t = 0.1$ and 0.7 for various interface conditions with $\delta x = 0.05$, $k_2 = 0.1$. $R_{bd} = 0$ represents the perfect contact interface.

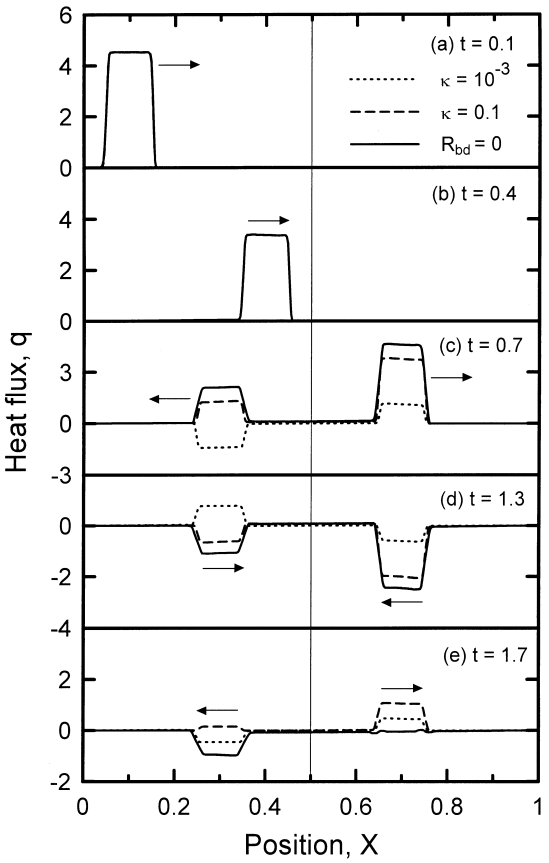

Fig. 3. Heat flux distributions at a sequence of times for various interface conditions with $\delta x = 0.05$, $k_2 = 10$. $R_{bd} = 0$ represents the perfect contact interface.

based on the updated interface heat flux, new iterations for T and q values of layer 2 are obtained. The procedure is repeated until the T and q values in the composite media are valid for the criterion of convergence

$$\left|\frac{T - T^{\text{iter}}}{T}\right|_{\max} \le 10^{-5} \text{ and } \left|\frac{q - q^{\text{iter}}}{q}\right|_{\max} \le 10^{-5} \qquad (24)$$

Then, the new values of T and q of both layers at the time $(n+1)$ can be evaluated.

4. Results and discussion

A one-dimensional computer code was written based on the above calculation procedure. Grid refinement and time step sensitivity studies were also performed for the physical model to ensure that the essential physics are independent of grid size and time interval. The pulsed incident energy is absorbed by skin depth δx. The emanating temperature in δx at $t = 0^+$ is inverse with skin depth for a constant incident energy. By choosing the $\varepsilon_d = 0.5$, we obtain

$$T = \begin{cases} \dfrac{1}{2\delta x}, & 0 \le x \le \delta x \\ 0, & \text{otherwise} \end{cases} \quad \text{for } t = 0^+ \qquad (25)$$

To simplify this task, the property ratios of α and τ of two layers are set to unity. In addition, layer 1 and layer 2 are assumed to be of equal length, and the total non-dimensional length is set to unity. In particular, for metal at the room temperature, the $\alpha \sim 10^{-4}$ m^2/s, $\tau \sim 10^{-12}$ s, $c \sim 10^5$ m/s [16], the physical space and time scales to correspond dimensionless $x = 1$ and $t = 1$ are in the order of 1 nm and 0.01 ps, respectively.

Fig. 2 illustrates the heat flux and temperature distribution for various interface conditions. The hyperbolic heat conduction equation predicts that a thermal wave disturbance tends to propagate in a given direction until the wall or barrier impedes its course. Initially,

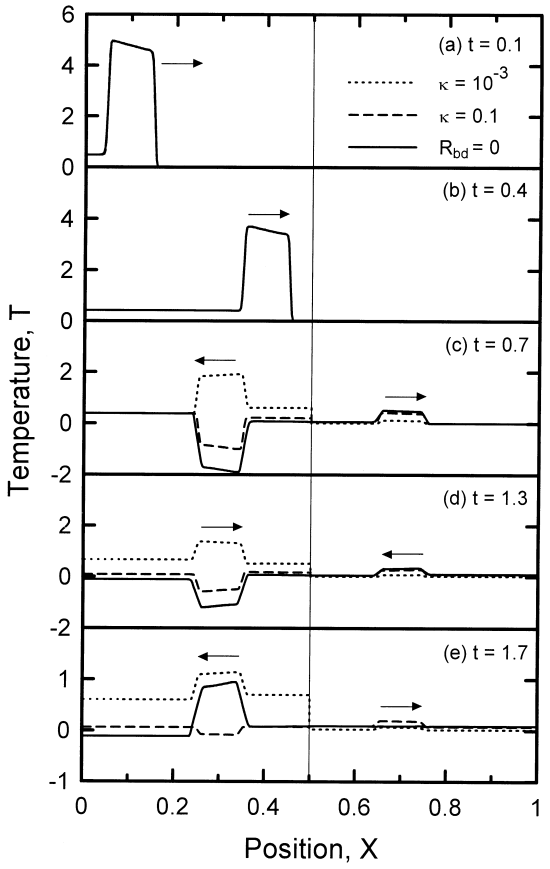

Fig. 4. Temperature distributions at a sequence of times for various interface conditions with $\delta x = 0.05$, $k_2 = 10$. $R_{bd} = 0$ represents the perfect contact interface.

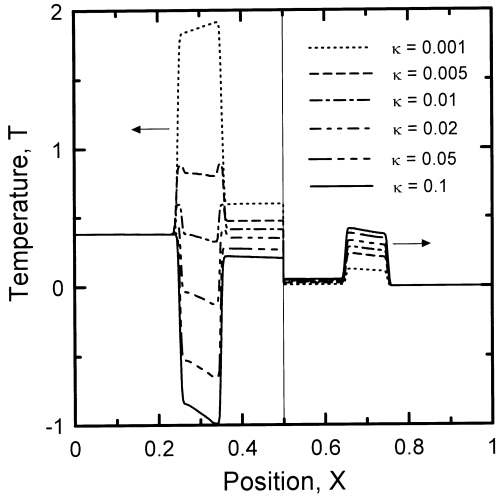

Fig. 5. Effect of interface condition on temperature at $t = 0.7$ with $\delta x = 0.05$, $k_2 = 10$.

owing to the reflection of the pulse wave from the insulated surface at $x = 0$, the wave width is doubled. This causes the leading edge of the wave front to impact at the contact interface and starts to reflect and transmit at $t = 0.45$. Before this occurs, the temperature and heat flux distributions are identical for each κ value, as attributed to that the wave front is unaware of the condition at the interface. At $t = 0.7$, the reflected wave travels towards the left and the transmitted wave travels towards the right; both waves retain the initial waveform. Since $k_2 < k_1$, the energy is restricted to transmit into layer 2 and most of the energy is reflected back to layer 1 even the contact interface is in perfect condition. With the interface resistance, the transmitted heat flux strength decreases with a decrease of κ. The opposite situation occurs for the heat flux in the reflected portion on the basis of energy conservation. For the temperature distribution, the heat capacity of ρC_p changes proportionally to k when α is held constant. Therefore, the discrepancies in induced temperature between different κ values in the transmitted portion are more significant than the reflected portion due to $k_2 < k_1$. In addition, the interface temperature continuity breaks down when thermal resistance exists. The temperature jump at the interface is attributed to the reduction of layer 2 interface temperature from the perfect contact value. Figs. 3 and 4 display the heat flux and temperature distribution, respectively, at various time intervals. By effect of diffusion, a small residual temperature in the wake of propagating wave, a slant across the top of wave and the waves strength attenuate with time are observed in Fig. 3(a) and (b) and Fig. 4(a) and (b). After the initial wave impact of the interface, Frankel et al. [21] indicated that $k_2 > k_1$ causes more energy to enter layer 2, thereby creating the negative reflected temperature wave based on the energy conservation for perfect contact interface. However, despite the transmitted energy ability of the environment is enhanced for $k_2 > k_1$, the reflected wave in Figs. 3(c) and 4(c) may be positive or negative in magnitude, depending on the interface condition. The temperature discrepancies between different κ values in reflected portion are more significant than those in transmitted portion due to $k_1 < k_2$. In addition, the temperature difference at the interface is attributed to the increase of layer 1 interface temperature from perfect contact value by the effect of thermal resistance. Bai and Lavine [23] used a jump temperature as the boundary condition of a thin layer to simulate the interface resistance. This treatment may not be satisfactory when $k_1 < k_2$. By $t = 1.3$, a pure reflection has occurred at the insulated external boundaries which do not allow the energy to be transmitted through the surfaces. Thus, the heat flux waves are converted into inverse wave front (Fig. 3(d)); temperature waves remain in the original wave front (Fig.

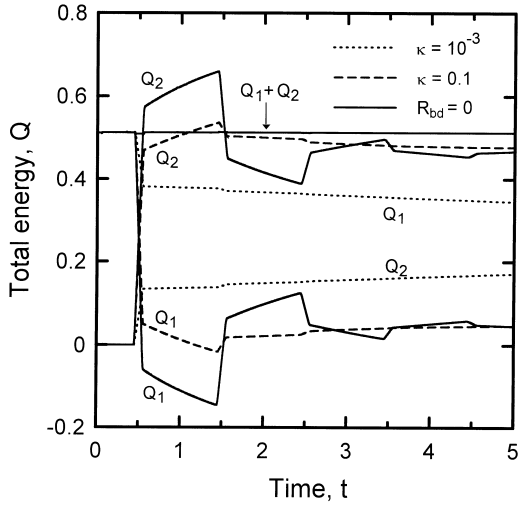

Fig. 6. Total energy versus time for various interface conditions with $\delta x = 0.05$, $k_2 = 10$. $R_{bd} = 0$ represents the perfect contact interface.

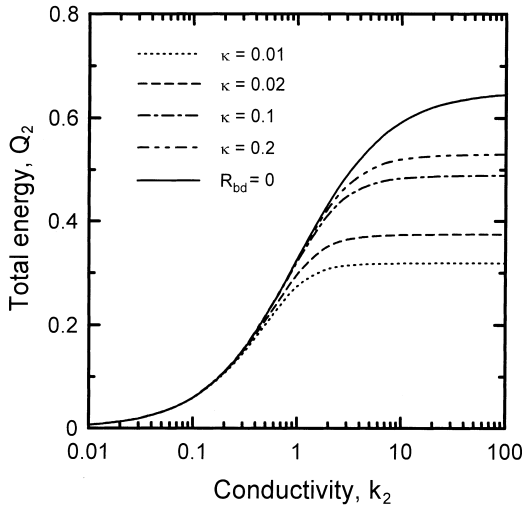

Fig. 7. Total energy of layer 2 at $t = 0.7$ vs. k_2 for various interface conditions with $\delta x = 0.05$. $R_{bd} = 0$ represents the perfect contact interface.

4(d)) moving towards the interface. According to Figs. 3(e) and 4(e), the waves impact the interface again by $t = 1.7$. This impact appears to combine the two waves emanating from different layers ultimately forming a single wave moving towards the origin for a perfect contact interface [21]. However, the reflection and transmission phenomena occur again when thermal resistance exists at the interface. The reflection–transmission combination persists until diffusion dominates in both layers.

Fig. 5 presents the temperature distribution for various interface conditions at $t = 0.7$. The temperature difference at interface which increases with a decrease of κ is owing to that less energy is transmitted into layer 2 for lower κ values. In the reflected portion, our results indicate the transition of the reflected waves from negative sign to positive sign with the variation of κ value. Herein, the wave consisting of a dimensionless temperature lower than the initial value of 0 is designated as a negative wave. The reflected wave changes its sign from a negative sign at $\kappa = 0.02$ to a positive one when the resistance magnitude reaches a κ value of 0.01. This finding implies that the interface resistance is equivalent to reducing the transmit energy ability of the environment. The transmit energy ability of the environment at $k_2 = 10$ is equivalent to reducing to $k_2 = 1$ at $\kappa = 0.01$, as evidenced by the fact that the reflected wave temperature is nearly the same as the residual value in the wake of propagating wave.

Fig. 6 illustrates the dimensionless total energy as time elapses for different values of κ. The total energy Q_1 and Q_2 can be obtained from the spatial integral of $\rho C_p T$ in the entire area of layer 1 and layer 2, respectively. The leading edge of the initial pulsed wave front impacts at the interface at $t = 0.45$. After a dimensionless time interval of 1, the waves reflected by the exterior insulated surfaces impact the interface again. At these moments, the total energy abruptly changes. For the remaining times, the total energy gradually changing with time is attributed to that the residual energy in the wake of propagating wave exchanges a slight amount of energy across the interface. The energy exchange between the two different layers heavily depends on the interface conditions. Our results clearly demonstrate that when the interface resistance is neglected, the Q_1 value which can represent the average temperature of layer 1 is significantly underestimated. Notably, owing to that the external boundaries are insulated for all time intervals, the total energy content in the composite media ($Q_1 + Q_2$) remains constant and equals the incident energy of 0.5. A situation in which Q_2 is greater than 0.5 implies not only that the total incident energy, but also that the initial internal energies of layer 1 are transmitted into layer 2. However, the extra energy gained from the internal energy of layer 1 is transmitted back to layer 1 when the waves are reflected by the exterior surfaces and impact the interface. Eventually, the Q_2 value is less than the total incident energy. In addition, the energy exchange decreases with time due to the effect of diffusion and the heat transfer across the interface is proportional to the difference of the fourth power of temperature on each side of the interface.

Fig. 7 depicts the relationship between total energy Q_2 and k_2 for different interface conditions to demonstrate the effect of k_2 and κ on the energy transmission. The Q_2 values are taken at $t = 0.7$. For a specified

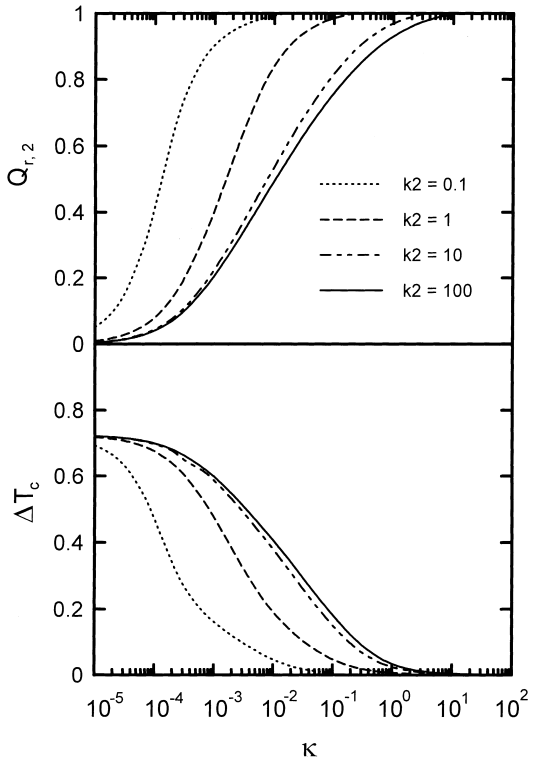

Fig. 8. Total energy ratio of layer 2 and temperature difference at interface at $t = 0.7$ versus interface conditions for various k_2 with $\delta x = 0.05$.

interface condition, increasing k_2 enhances the transmit energy ability of the environment. However, the induced temperature magnitude in layer 2 decreases with an increase of k_2, since the heat capacity of ρC_p changes in proportion to k when α is held constant. The limiting case is when the layer 2 temperature approaches zero for a sufficiently large k_2 value. Beyond this k_2 value, the Q_2 is independent of the variation of k_2 for each constant κ. This critical k_2 value increases with an increase of κ.

Fig. 8 illustrates the relationship between Q_{r2} and ΔT_c with κ at $t = 0.7$. Where Q_{r2} is the relative energy transmission ability, i.e., the ratio of the total energy transmitted across the resistance interface into layer 2 to the value across the perfect contact interface. In addition, ΔT_c denotes the temperature difference at interface, i.e., $T_{1c} - T_{2c}$. When Q_{r2} approaches unity, the interface is in a nearly perfect condition. In contrast, no energy can be transmitted across the interface when Q_{r2} approaches zero. Notably, the increasing rate of Q_2 with k_2 in perfect contact interface is reduced by resistance. Such a reduction causes the Q_{r2} to decrease with an increase of k_2 for a constant κ value. Moreover, the limiting κ value for approaching the perfect contact interface where $Q_{r2} \to 1$ and $\Delta T_c \to 0$ increases with an increase of k_2. The $Q_{r2} \to 0$ approaches the adiabatic interface when $\kappa \approx 10^{-5}$. Meanwhile, a high ΔT_c value is observed.

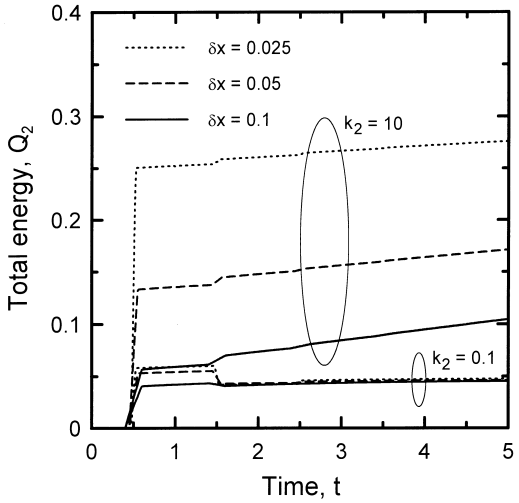

Fig. 9. Total energy of layer 2 versus time for various skin depth δx with $\kappa = 10^{-3}$.

This study also attempts to understand the influence of absorption skin depth δx under a fixed incident energy. Fig. 9 illustrates the Q_2 as time elapses for different values of δx. Owing to that a higher temperature wave is released in a thinner δx at $t = 0^+$, the Q_2 abruptly increases from zero to a value which increases with a decrease of δx at the moment when the initial pulsed wave impacts the interface. After time interval of 1, the waves reflected from exterior adiabatic sur-

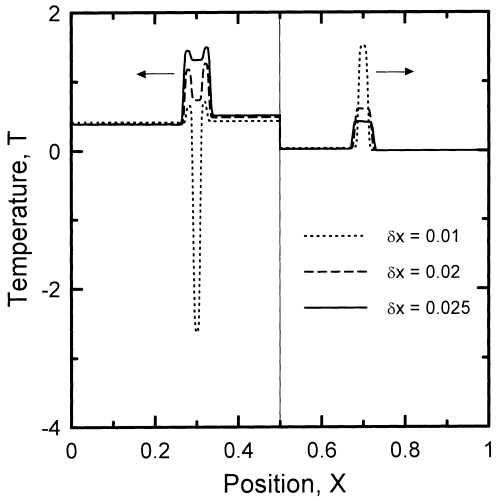

Fig. 10. Effect of skin depth δx on temperature at $t = 0.7$ with $k_2 = 10$, $\kappa = 10^{-3}$.

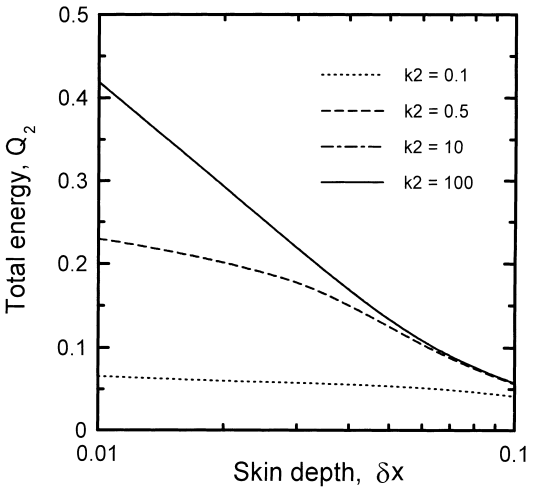

Fig. 11. Effect of skin depth δx on total energy of layer 2 at $t = 0.7$ for various k_2 with $\kappa = 10^{-3}$.

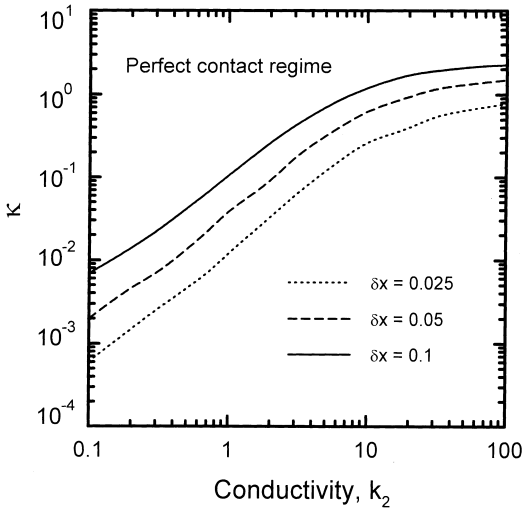

Fig. 12. Regime map of perfect contact interface for various skin depth δx.

faces impact the interface again. At this moment, the energy transmits back to layer 1 for $k_2 = 0.1$, which is in contrast to the occurrence for $k_2 = 10$ that layer 2 gain more energy. The effect of diffusion and energy transmission weakens the wave strength. Thereafter, the energy does not abruptly change when the waves impact the interface.

Fig. 10 presents the temperature distribution at $t = 0.7$ for three different δx. The different energy transmitted across the interface into layer 2 for different δx indicates that the equivalent k_2 varies with δx. The transmission energy across the interface restricted by the thermal resistance with a κ value of 10^{-3} is equivalent to reducing the $k_2 = 10$ to a value greater than unity for $\delta x = 0.01$, which reflects a negative sign wave and to the values less than unity for $\delta x = 0.02$ and 0.025, which reflects the positive sign waves. In addition, the temperature difference at the interface increases with δx, which corresponds to a decrease of the energy transmission across the same interface condition with an increase of δx.

Fig. 11 illustrates the energy consisting of layer 2 at $t = 0.7$ varied with δx. For the same interface condition, the energy transmit across the interface depends on the initial pulsed temperature strength which is related to δx, and the transmit energy ability of the environment which is related to k_2. Due to the weak transmit energy ability of the environment when k_2 is small, the energy discrepancies between the different skin depths is insignificant. In addition, for a large δx in which an initial pulsed temperature strength is weak, the energy discrepancies between the different k_2 are less significant than those for a small δx. Notably, the relationship of energy transmission to δx for $k_2 = 10$ is the same as that with $k_2 = 100$, indicating that $k_2 = 10$ is greater than the critical k_2 value at $\kappa = 10^{-3}$. Beyond this value, the total energy in layer 2 is independent of the variation of k_2 for each κ value, as described earlier in Fig. 7.

Fig. 12 presents the regime map for the perfect contact interface for different δx. For an individual k_2, when the energy across the interface with a resistance magnitude κ is 95% of the value across the perfect contact interface, then the critical κ which approaches the perfect contact interface is obtained. The total energy value in layer 2 at time $t = 0.7$ is adopted to asses the energy across the interface. When the interface resistance magnitude κ is above the loci, the effect of the resistance is negligible. Consequently, the interface can be treated as a perfect condition. On the other hand, the effect of the interface resistance should be considered when the resistance magnitude κ is below the loci. Notably, even if the interface is in perfect condition, only a slight amount of energy can be transmitted into layer 2 when k_2 is sufficiently small. This accounts for why the discrepancy between the energy across perfect contact interface and across resistance interface is relatively minor. Thus, for a small k_2, the interface can be treated as a perfect condition even with a heavy resistance interface (small κ value). With a constant absorption skin depth, the critical κ to approach the perfect contact interface increases with the conductivity ratio of layer 2 to layer 1. In addition, owing to that the transmitted energy is inversely proportional to the skin depth, the critical κ value to approach the perfect contact case increases with the absorption skin depth when the conductivity ratio is held constant.

5. Conclusions

By applying hyperbolic heat conduction, this study analyzes how the interface thermal resistance affects the thermal wave propagation in a two-layered composite media. The radiation heat flux model (either AMM or DMM) is used to examine the interface thermal resistance.

The reflection and transmission occur when the initial pulse wave impacts the contact surface of dissimilar materials. In addition, the thermal resistance restricts the exchanges of energy between two dissimilar layers, ultimately creating a temperature difference at the interface. The temperature difference at interface is attributed to the reduction layer 2 interface temperature from perfect contact value when $k_2 < k_1$. In contrast, layer 1 interface temperature arises from perfect contact value when $k_2 > k_1$. The relative strengths of reflected wave and transmitted wave varies with the interface conditions, two-layered property ratio, and the absorption skin depth. Although the energy transmitted across the interface significantly increases with the decrease of the absorption skin depth when $k_2 > k_1$, it is not significantly affected by the variation of skin depth when $k_2 < k_1$.

Analysis results further demonstrate that thermal resistance not only mediates the energy transform from one layer to the other, but also markedly influences the thermal wave transmission–reflection-combination phenomena. The negative wave, which is reflected by the perfect contact interface when $k_2 > k_1$, may change its sign when considering the interface resistance. Moreover, the effect of the thermal resistance can be neglected when the resistance magnitude is beyond a critical value. The critical resistance magnitude to approach the perfect contact condition increases with the absorption skin depth and conductivity ratio of k_2 to k_1.

Acknowledgements

The authors would like to thank the National Science Council of Taiwan, R.O.C. for financially supporting this research under Contract No. NSC 88-2218-E-009-003. Dr. J.P. Wu is also appreciated for his valuable discussions.

References

[1] M.I. Flik, P.E. Phelan, C.L. Tien, Thermal model for the bolometric response of high T_c superconducting films to optical pulses, Cryogenics 30 (1990) 1118–1128.
[2] R.C. Chen, J.P. Wu, H.S. Chu, Bolometric response of high-T_c superconducting detectors to optical pulses and continuous waves, ASME J. Heat Transfer 117 (1995) 366–372.
[3] P.E. Phelan, Application of diffuse mismatch theory to the prediction of thermal boundary resistance in thin-film high-Tc superconductors, ASME J. Heat Transfer 120 (1998) 37–43.
[4] B. Bertman, D.J. Sandiford, Second sound in solid helium, Scientific American 222 (1970) 92–101.
[5] M.J. Maurer, H.A. Thompson, Non-Fourier effects at high heat flux, ASME J. Heat Transfer 95 (1973) 284–286.
[6] D.Y. Tzou, On the thermal shock wave induced by a moving heat source, ASME J. Heat Transfer 111 (1989) 232–238.
[7] A. Vedavarz, S. Kumar, M.K. Moallemi, Significance of non-Fourier heat waves in conduction, ASME J. Heat Transfer 116 (1994) 221–224.
[8] C. Cattaneo, Sullaconduzione de calore, in: Atti del Seminar, vol. 3. Mat. Fis. Univ., Modena, 1948, pp. 83–101.
[9] P. Vernotte, Les paradoxes de la theorie continue de l'equation de la chaleur, Compute Rendus 246 (1958) 3145–3155.
[10] M. Chester, Second sound in solid, Physical Review 131 (1963) 2013–2015.
[11] D.D. Joseph, L. Preziosi, Heat wave, Review of Modern Physics 61 (1989) 41–73.
[12] K. Mitra, S. Kumar, A. Vedavarz, M.K. Moallemi, Experimental evidence of hyperbolic heat conduction in processed meat, ASME J. Heat Transfer 117 (1995) 568–573.
[13] D.Y. Tzou, Macro- to Microscale Heat Transfer: The Lagging Behavior, Taylor and Francis, Washington, DC, 1996.
[14] G. Chen, Phonon wave effects on heat conduction in thin films, AIAA/ASME Joint Thermophysics and Heat Transfer Conference 3 (1998) 205–213.
[15] T.Q. Qiu, C.L. Tien, Short-pulse laser heating on metals, Int. J. Heat Mass Transfer 35 (1992) 719–726.
[16] D.Y. Tzou, The generalized lagging response in small-scale and high-rate heating, Int. J. Heat Mass Transfer 38 (1995) 3231–3240.
[17] A. Majumdar, Microscale heat conduction in dielectric thin films, ASME J. Heat Transfer 115 (1993) 7–16.
[18] C. Bai, A.S. Lavine, Hyperbolic heat conduction in a superconducting film, in: ASME/JSME Thermal Engineering Proceedings, vol. 3, 1991, pp. 87–92.
[19] D.E. Glass, M.N. Özisik, W.S. Kim, Formulation and solution of hyperbolic Stefan problem, J. Applied Physics 70 (1987) 1190–1197.
[20] M.N. Özisik, D.Y. Tzou, On the wave theory in heat conduction, ASME J. Heat Transfer 116 (1994) 526–535.
[21] J.I. Frankel, B. Vick, M.N. Özisik, General formulation and analysis of hyperbolic heat conduction in composite media, Int. J. Heat Mass Transfer 30 (1987) 1293–1305.
[22] D.Y. Tzou, Reflection and refraction of thermal waves from a surface or an interface between dissimilar materials, Int. J. Heat Mass Transfer 36 (1993) 401–410.
[23] C. Bai, A.S. Lavine, Thermal boundary conditions for

hyperbolic heat conduction, in: Heat Transfer on the Microscale. ASME 1993, HTD-vol. 253, 1993, pp. 37–44.
[24] A.E. Kronberg, A.H. Benneker, K.R. Westerterp, Notes on wave theory in heat conduction: a new boundary condition, Int. J. Heat Mass Transfer 41 (1998) 127–137.
[25] W.A. Little, The transport of heat between dissimilar solid at low temperature, Can. J. Phys 37 (1959) 334–349.
[26] E.T. Swartz, R.O. Pohl, Thermal boundary resistance, Reviews of Modern Physics 61 (1989) 605–668.
[27] J.F. Gibbons, L.D. Hess, T.W. Sigman, Laser and Electron-Beam Solid Interactions and Material Processing, Elsevier/North Holland, New York, 1981.
[28] B.R. Appleton, G.K. Cellar, Laser and Electron-Beam Interactions with Solids, Elsevier Science, New York, 1982.
[29] I.W. Boyd, Laser Processing of Thin Films and Microstructures, Springer, New York, 1989.
[30] G. Chryssolouris, Laser Machining, Theory and Practice, Springer, New York, 1991.
[31] H.Q. Yang, Characteristics-based, high-order accurate and nonoscillatory numerical method for hyperbolic heat conduction, Numer. Heat Transfer B 18 (1990) 221–241.
[32] W.K. Yeung, T.T. Lam, A numerical scheme or non-Fourier heat conduction. Part I: one-dimensional problem formulation and applications, Numer. Heat Transfer B 33 (1998) 215–233.